Journal of Microscopy, Vol. 200, Pt 1, October 2000, pp. 68–74.
Received 20 March 2000; accepted 6 June 2000

Strategies for the compensation of specimen-induced spherical aberration in confocal microscopy of skin

M. J. BOOTH & T. WILSON
Department of Engineering Science, University of Oxford, Parks Road, Oxford OX1 3PJ, U.K.

Key words. Aberration correction, confocal microscopy, skin.

Summary

We consider various strategies for confocal imaging of human skin which seek to reduce the effects of the specimen-induced aberrations. We calculate the spherical aberration introduced by the stratified structure of skin and show how the confocal signal is affected when attempting to image at various depths within the dermis. Using simple methods it is shown how images might be improved by compensating for the induced aberration. The methods include the use of an iris to reduce the pupil area, changing the refractive index of the immersion medium and using a lens with variable coverglass correction.

Introduction

The main advantage of the confocal microscope lies in its ability to image efficiently only those regions of an object which lie close to the focal plane. This optical sectioning ability permits through-focus series of optical slices to be recorded, which can then be processed to render the volume object in any required fashion (Wilson & Sheppard, 1984; Wilson, 1990; Pawley, 1995). A fundamental desire for a confocal microscope is therefore the ability to produce high quality diffraction limited images deep within a real specimen. This requirement is at odds with many standard microscope objective lenses that are designed, for example, to image thin objects located directly under a glass cover slip of specified thickness. Spherical aberration may be introduced due to refractive index mismatch between the immersion medium (or air) and the specimen. The effects of this on the performance of confocal microscopes have been investigated by several researchers (see, e.g. Hell *et al.*, 1993; Török *et al.*, 1997). Aberrations could be removed, in principle, by measuring the wavefront distortion and adaptively conditioning the probe beam with an equal and opposite aberration (Booth *et al.*, 1998; Neil *et al.*, 2000). Several static methods of aberration compensation have been proposed, for example, by altering the tube length of the objective (Sheppard & Gu, 1991), or by choosing an immersion medium which minimizes the overall aberration (Wan *et al.*, 2000). However, there are many practical cases in which it is impossible to employ such methods.

We consider alternative strategies for aberration correction. As a specific example we place our discussion in the context of imaging deep into human skin (Rajadhyaksha *et al.*, 1999), which we model as a multilayer structure. We discuss the practical tradeoffs that are necessary when imaging features located deep within the dermis.

Correspondence: M. J. Booth. E-mail: martin.booth@eng.ox.ac.uk

The confocal response

The pupil plane of an objective lens is uniformly illuminated by light of free space wavelength λ. In this pupil plane there is a circular aperture of radius a (see Fig. 1). The focus of this objective lies in a medium with refractive index n. The confocal image of a point object located in the focal plane can be calculated as (Wilson & Sheppard, 1984)

$$I(r) = \left| \frac{2\pi n}{\lambda f} \int_0^a P'(r') J_0\left(\frac{2\pi n r' r}{\lambda f}\right) r' \mathrm{d}r' \right|^4 \qquad (1)$$

where r is the radial distance, f is the focal length of the lens, $J_0(.)$ is the zeroth order Bessel function of the first kind, $P'(.)$ is the pupil function of the lens, and r' is the radial coordinate in the pupil plane. The pupil function can be used to describe any aberrations introduced into the system by the specimen. It is convenient to use a normalized coordinate system in the pupil plane so that the integration is always performed over a unit circle even if the actual pupil size changes. We therefore make the following substitution in Eq. (1):

$$r' = \rho a \qquad (2)$$

We also introduce the coordinate v in the focal plane where (Wilson & Sheppard, 1984)

$$v = \frac{2\pi n a r}{\lambda f} \qquad (3)$$

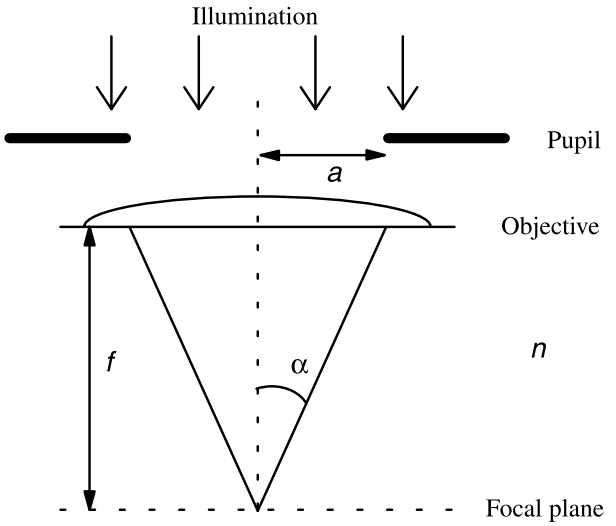

Fig. 1. Schematic showing the focusing geometry of the objective lens. The adjustable circular pupil has radius a and is illuminated by a constant power density.

Equation (1) then becomes:

$$I(r) = \left|\frac{2\pi n a^2}{\lambda f}\int_0^1 P(\rho)J_0(\rho v)\rho \mathrm{d}\rho\right|^4 \tag{4}$$

where $P(\rho) = P'(\rho\alpha)$. This normalization ensures that when there is no aberration, i.e. $P(\rho) = 1$, and the point object is on-axis, i.e. $r = 0$, the integral returns the same value regardless of the pupil radius, a. It follows that when the illumination of the pupil plane is constant, the maximum intensity of the confocal signal for no aberration is proportional to the fourth power of the pupil area, which is given by $A = \pi a^2$:

$$I(r) = A^4\left|\frac{2n}{\lambda f}\int_0^1 P(\rho)J_0(\rho v)\rho \mathrm{d}\rho\right|^4 \tag{5}$$

As it is usually the numerical aperture (NA) of the lens which is specified, rather than the pupil area, we can calculate A from the relationship

$$A = \pi f^2 \tan^2\alpha = \pi f^2 \frac{NA^2}{n^2 - NA^2} \tag{6}$$

where α is the semi-aperture angle of the objective lens and $NA = n\sin\alpha$. We also note that v can be written in terms of α:

$$v \approx \frac{2\pi n r}{\lambda}\sin\alpha \tag{7}$$

Equation (5) describes the confocal signal from a point object situated in the focal plane. When the point lies in a plane a distance z away from the focal plane we include a quadratic phase term in the integral (Wilson & Sheppard, 1984):

$$I(r,z) = A^4\left|\frac{2n}{\lambda f}\int_0^1 P(\rho)\exp\left(\frac{ju\rho^2}{2}\right)J_0(\rho v)\rho \mathrm{d}\rho\right|^4 \tag{8}$$

where the coordinate u is related to the real distance z by (Wilson & Sheppard, 1984)

$$u = \frac{8\pi n z}{\lambda}\sin^2\left(\frac{\alpha}{2}\right) \tag{9}$$

Thus Eq. (8), in conjunction with Eqs (6), (7) and (9), allows us to calculate the confocal response to a point object situated anywhere in the focal region of an objective lens for different pupil sizes and hence different numerical apertures. Any aberrations that are present in the system can be represented by the pupil function $P(\rho)$.

The pupil function

The optical properties of the external part of human skin can be reasonably approximated by a three-layered structure consisting of the stratum corneum, the epidermis and the dermis. The refractive indices of each layer have been accurately determined using optical coherence tomography (Tearney *et al.*, 1995) and are found to be 1.51, 1.34 and 1.40, respectively. When light is focused into skin using a microscope objective with the appropriate immersion medium, the light travels as a spherical wavefront from the objective to the surface of the skin. If the refractive index of the immersion medium differs from that of the adjacent layer then spherical aberration is introduced into the wavefront and its shape departs from the ideal spherical form. This process occurs again at each interface in the stratified medium, adding further aberration. The focusing geometry we consider is shown in Fig. 2, where the focus of the objective lies in the dermis, and thus there are three

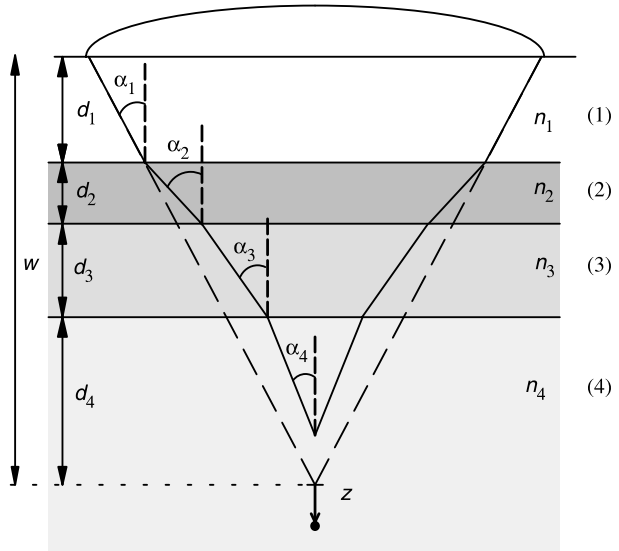

Fig. 2. Schematic diagram of the focusing geometry for the confocal imaging of skin. Layer (1) is the lens immersion medium. The skin is approximated by the three-layer structure shown, consisting of (2) the stratum corneum (3) the epidermis, and (4) the dermis.

refractive index interfaces where spherical aberration is introduced. We have shown previously (Booth *et al.*, 1998) that the spherical aberration introduced at such an interface can be modelled as a phase function in the pupil plane of the lens; when focusing a depth d into a medium of refractive index n_2 from a medium of refractive index n_1, the phase aberration is given by

$$\Psi(\rho) = \frac{2\pi}{\lambda} d n_1 \sin\alpha_1 \left[\sqrt{\csc^2\alpha_2 - \rho^2} - \sqrt{\csc^2\alpha_1 - \rho^2}\right] \tag{10}$$

where ρ is the radial coordinate in the pupil plane, normalized such that the pupil has unity radius. α_1 is the semi-aperture angle of the objective lens and α_2 is found using Snell's law: $n_1 \sin\alpha_1 = n_2 \sin\alpha_2$. We can extend this analysis to calculate the aberrations when focusing into multiple layers. If there are P layers in total and the pth layer has thickness d_p and refractive index n_p, the total phase aberration is given by

$$\Psi(\rho) = \frac{2\pi}{\lambda} n_1 \sin\alpha_1 \sum_{p=1}^{P} d_p \left[\sqrt{\csc^2\alpha_2 - \rho^2} - \sqrt{\csc^2\alpha_1 - \rho^2}\right] \tag{11}$$

where the angle α_p is again found using Snell's law: $n_1 \sin\alpha_1 = n_p \sin\alpha_p$. We also note that $n_1 \sin\alpha_1$ is simply the NA of the objective lens. The corresponding pupil function is therefore given by

$$P(\rho) = \exp\{j\Psi(\rho)\} \tag{12}$$

Confocal imaging of the dermis

We will assume that the objective lens is positioned a distance d_1 from the surface of the skin and is used together with an index matching medium of refractive index n_1. The skin is modelled, as we have said, as a three-layer structure consisting of the stratum corneum (with refractive index $n_2 = 1.51$ and thickness $d_2 = 10$ μm), the epidermis (with refractive index $n_3 = 1.34$ and thickness $d_3 = 150$ μm) and the dermis (refractive index $n_4 = 1.41$). The nominal focal plane (NFP) is taken to be at a distance d_4 below the epidermal–dermal junction, a total distance of w from the objective lens. This is the distance at which the focus would lie if the refractive index of the object were matched to the immersion medium; w is usually called the working distance of the lens. We probe the effective confocal distribution by considering a point object located at a radial distance r from the optical axis and displaced axially by a distance z from the NFP. Omitting constant multiplying factors, Eq. (8) becomes

$$I(r,z) = A^4 \left| \int_0^1 P(\rho) \exp\left(\frac{ju\rho^2}{2}\right) J_0(\rho v) \rho \mathrm{d}\rho \right|^4 \tag{13}$$

with

$$A = \tan^2\alpha_1 = \frac{NA^2}{n_1^2 - NA^2} \tag{14}$$

$$v = \frac{2\pi n_4 r}{\lambda} \sin\alpha_4 = \frac{2\pi}{\lambda}(NA) r \tag{15}$$

$$u = \frac{8\pi n_4 z}{\lambda} \sin^2\left(\frac{\alpha_4}{2}\right) \tag{16}$$

Some objective lenses have an iris incorporated in the pupil plane to allow the user to choose the aperture size and hence control the NA of the lens. This can also be achieved by the use of an iris suitably located elsewhere in the system. As the magnitude of the phase aberration is greatest at the periphery of the pupil plane, it may be desirable to reduce the size of the pupil and hence the amount of spherical aberration. This of course also reduces the amount of light passing through the pupil, in both the illumination and emission paths, as has been taken into account in the derivation of Eq. (13).

Discussion

We now look at the effects of using the iris to reduce the pupil size (effective NA) when focusing to a certain depth in the dermis. The specifications of the lenses we consider are typical of those currently commercially available. For all the following examples we take the wavelength of the illumination to be $\lambda = 830$ nm. First we consider a dry lens with a nominal NA of 0.6 and working distance $w = 0.9$ mm which is focused to a nominal depth of $d_4 = 200$ μm below the epidermal–dermal junction. The point object is located on the optical axis at an axial distance z from the NFP. Figure 3 shows how the axial distribution of the confocal signal is affected by the reduction of the pupil size (plotted as a function of NA). All figures are normalized to the maximum intensity. It can be seen that when the lens is used with the maximum NA possible, i.e. 0.6, the axial distribution is heavily distorted due to the spherical aberration induced by the specimen. There are also significant side lobes present. However, if the NA is reduced to around 0.43 we find that the axial distribution has a narrower and more regular shape without significant side lobes, although the peak intensity is reduced to around 60% of the peak intensity when the NA is 0.6. We also note that the axial position of the peak intensity for low NA is close to that predicted by paraxial ray tracing, $z = 140$ μm. In some microscopes it may be possible to adjust the expansion of the illumination beam so that an equal amount of light passes through the pupil even when the size of the pupil is altered. The axial distributions for this case are shown in

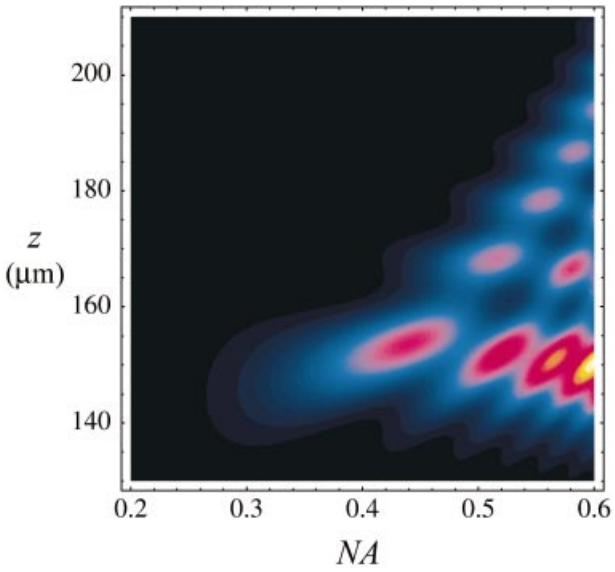

Fig. 3. Confocal response to an on-axis point object as a function of numerical aperture for a dry lens of maximum NA = 0.6. The depth $d_4 = 200$ μm. The colour table shows signal level normalized to the maximum value in this plot.

Fig. 4. The reduction of the NA now results in the same increase in focal spot quality but also a large increase in peak intensity. It should be noted that the maximum value in Fig. 4 is 2.5 times larger than the maximum in Fig. 3.

The spherical aberration induced when using a water immersion objective is much smaller than those in the previous dry lens case due to the closer matching of refractive indices between the immersion medium and the skin. In Figs 5(a) to (c) we show the axial distributions when focusing to depths of 100, 200 and 300 μm into the dermis using a water immersion objective with a nominal NA of 0.9. The NA is controlled by adjusting the pupil size and there is no alteration of the beam expansion. The peak intensities shown on the plots (a), (b) and (c) correspond to 0.11, 0.05 and 0.025, respectively. Figure 6 shows the equivalent results when using this lens to focus into a perfectly matched, aberration free medium; the peak intensity shown is 0.51. The axial distribution in this case reduces to

$$I(0,z) \propto A^4 \left[\frac{\sin(u/4)}{(u/4)}\right]^4 \qquad (17)$$

In the first case, Fig. 5(a), we notice that the distribution is broader than in the aberration free case but there are no significant side lobes. Focusing to a depth of $d_4 = 200$ μm we see that the shape of the axial distribution degrades at higher NA and there is a reduction in the intensity. These effects are further exaggerated at a focusing depth of $d_4 = 300$ μm. In these examples we again notice that the quality of the focal distribution may be increased by reducing the NA although the signal strength also reduces. We illustrate this further in Fig. 7, where we show cross-sections of the point spread functions (PSF) obtained when focusing to $d_4 = 200$ mm (as in Fig. 5b). Figure 7(a) shows the PSF obtained when the pupil is stopped down to an NA of 0.77, whereas Fig. 7(b) corresponds to the maximum NA of 0.9.

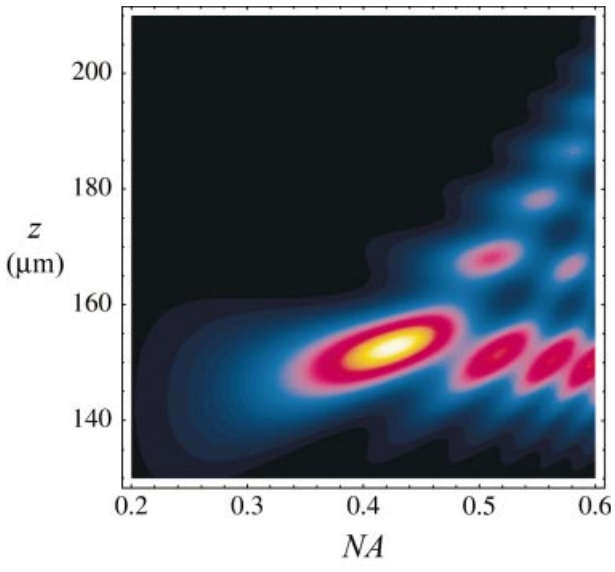

Fig. 4. Confocal response to an on-axis point object as a function of numerical aperture for a dry lens of maximum NA = 0.6. The depth $d_4 = 200$ μm. The illumination has been adjusted so that the same total power passes through the pupil for all NA.

Refractive index dependence

It is common practice to try to match the refractive index of the lens immersion medium to that of the sample in order to reduce the induced spherical aberration. With a multilayer medium such as skin, index matching is more difficult because each layer has different optical properties. If however, one were able to choose any refractive index for the immersion medium, it would be possible, for a given focusing situation, to find the optimum value. If the immersion medium is not the same as that for which the lens was designed then the medium can be treated as an extra aberrating layer. This is accommodated by the inclusion of an extra term in Eq. (11). We present an example of this in Fig. 8 using the water immersion lens described above at a focusing depth $d_4 = 200$ mm. The working distance of the lens is 2 mm. The results show that the optimum refractive index of the immersion medium for this configuration is approximately 1.32 and not the value of 1.33 for which the lens was designed. Also, using a large working distance lens such as this results in high sensitivity to changes in refractive index.

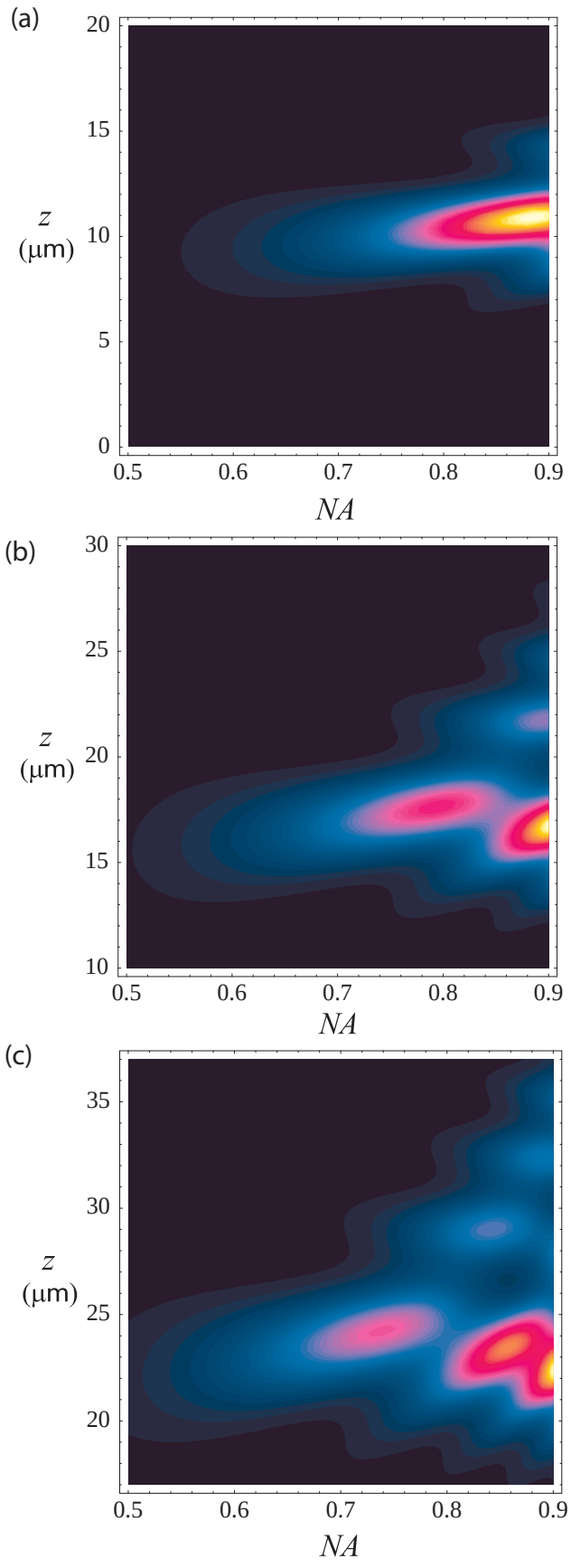

Consequently, the refractive index changes due to temperature or dissolved substances could be significant. For example, the refractive index of water decreases by 0.0025 between 18 °C and 38 °C (Weast, 1989). As an example of dissolved substances, the index of a sucrose solution in water increases by 0.003 as the concentration changes from 0 to 2% (Weast, 1989).

Coverglass correction

As we have said, some objective lenses incorporate optics which allow correction of the aberrations introduced by coverglasses of differing thickness. The degree of correction, corresponding to the thickness of coverglass, is usually controlled by means of a collar on the lens body. The correction optics function by effectively introducing an aberration equal but opposite to that induced by the coverglass. Using such a lens without a coverglass one can partially correct for the aberrations introduced by the layers of skin. The 'negative' correction aberration can be included in our analysis by introducing an extra term in Eq. (11) so that it becomes

$$\Psi(\rho) = \frac{2\pi}{\lambda} n_1 \sin\alpha_1 \left[\sum_{p=1}^{P} d_p \left[\sqrt{\csc^2\alpha_p - \rho^2} - \sqrt{\csc^2\alpha_1 - \rho^2} \right] - d_{cg} \left[\sqrt{\csc^2\alpha_{cg} - \rho^2} - \sqrt{\csc^2\alpha_1 - \rho^2} \right] \right] \tag{18}$$

where d_{cg} is the thickness of the absent coverglass and α_{cg} is found from the refractive index of the absent coverglass using $n_1 \sin\alpha_1 = n_{cg} \sin\alpha_{cg}$. Results in Fig. 9 show the axial response using a 0.9 NA water immersion lens for three different nominal focusing depths as a function of d_{cg}. The correction collar for this lens is designed to compensate for cover slips with thicknesses ranging from 130 μm to 250 μm. Adjusting the correction collar for a particular imaging depth, it is possible to create a significant increase in intensity and a better focal distribution than using an uncorrected lens. The maximum intensities in these three plots are approximately 20 times larger than those using a lens without correction. Many objectives are designed for a fixed coverglass thickness of typically 170 μm. Although only optimally corrected for one imaging depth, such a lens would still provide partial correction over a range of depths.

Fig. 5. Confocal response to on-axis point objects as a function of numerical aperture for a water immersion lens of nominal NA = 0.9 at different focusing depths: (a) $d_4 = 100$ μm; (b) $d_4 = 200$ μm; (c) $d_4 = 300$ μm.

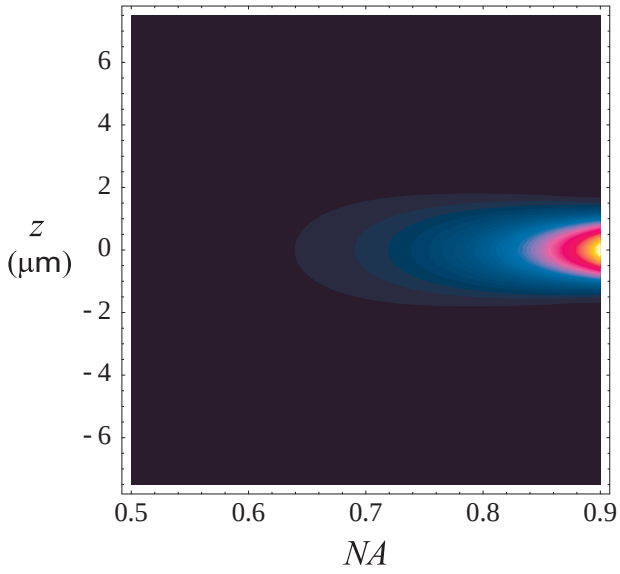

Fig. 6. Confocal response to an on-axis point object in a refractive index matched medium ($n = 1.33$) as a function of numerical aperture for a water immersion lens of nominal NA = 0.9.

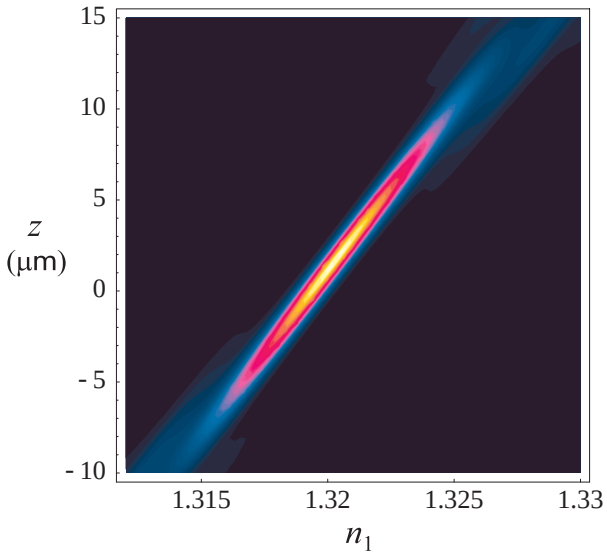

Fig. 8. Confocal axial response for focusing with an NA = 0.9 water immersion lens to a depth $d_4 = 200$ μm. The immersion medium used has a refractive index n_1 as shown on the horizontal axis.

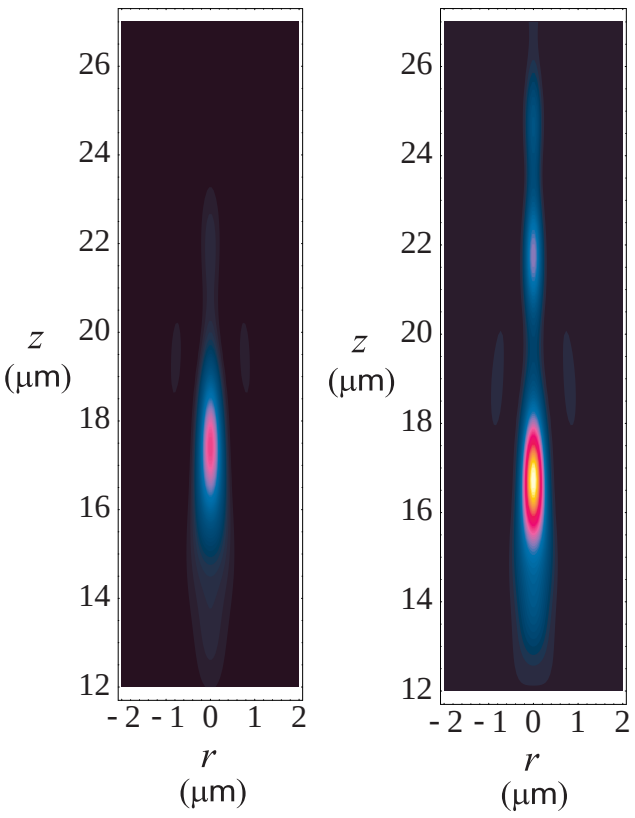

Fig. 7. Confocal point spread function cross-section plots using a water immersion lens focusing at a nominal depth $d_4 = 200$ μm for (a) NA = 0.77 and (b) NA = 0.9.

Conclusion

We have calculated the spherical aberration caused by imaging through multiple layers of differing refractive index and expressed it as a phase function in the pupil plane of an objective lens. This aberration is dependent upon various factors, the modification of which can lead to an improvement in imaging quality. Using an idealized model of human skin, we have considered the effects of specimen-induced aberrations for confocal imaging into the dermis. We have shown that by simply reducing the pupil size of the objective one is able to improve the focal distribution, although this is accompanied by a loss in overall signal. The refractive index of the immersion medium may be changed in order to partially compensate for the induced aberration. Certain imaging configurations, namely with high NA, large working distance lenses, may be especially sensitive to the refractive index of the immersion medium. Some objective lenses are designed for use with microscope coverglasses of different thicknesses. When such a lens is used to image skin without a coverglass, the variable correction allows vastly improved signal strength and resolution over a range of depths.

References

Booth, M.J., Neil, M.A.A. & Wilson, T. (1998) Aberration correction for confocal imaging in refractive index mismatched media. *J. Microsc.* **192**, 90–98.

Hell, S.W., Reiner, G., Cremer, C. & Stelzer, E.H.K. (1993)

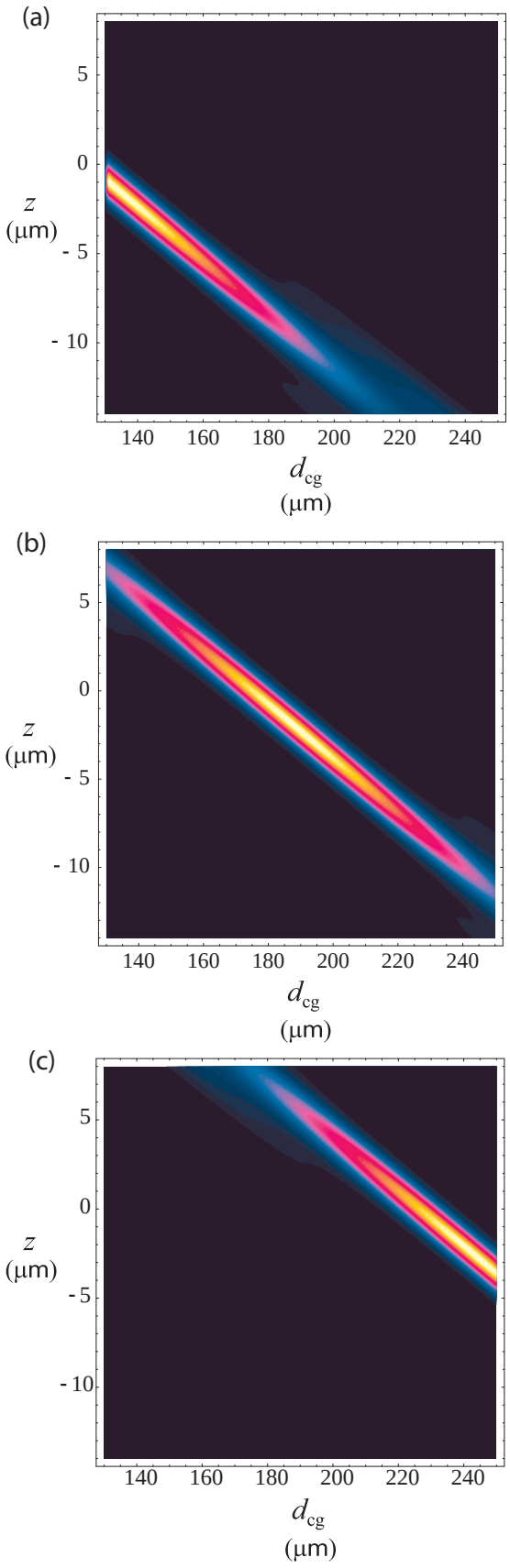

Aberrations in confocal fluorescence microscopy induced by mismatches in refractive index. *J. Microsc.* **169**, 391–405.

Neil, M.A.A., Wilson, T. & Juškaitis, R. (2000) A wavefront generator for complex pupil function synthesis and point spread function engineering. *J. Microsc.* **197**, 219–223.

Pawley, J.B., ed. (1995) *Handbook of Biological Confocal Microscopy.* Plenum, New York.

Rajadhyaksha, M., Gonzalez, S., Zavislan, J.M., Anderson, R.R. & Webb, R.H. (1999) *In vivo* confocal scanning laser microscopy of human skin II: advances in instrumentation and comparison with histology, *J. Invest. Dermatol.* **113**, 293–301.

Sheppard, C.J.R. & Gu, M. (1991) Aberration compensation in confocal microscopy. *Opt. Commun.* **88**, 180–190.

Tearney, G.J., Brezinski, M.E., Southern, J.F., Bouma, B.E., Hee, M.R. & Fujimoto, J.G. (1995) Determination of the refractive index of highly scattering human tissue by optical coherence tomography. *Opt. Lett.* **20**, 2258–2260.

Török, P., Hewlett, S.J. & Varga, P. (1997) The role of specimen induced spherical aberration in confocal microscopy. *J. Microsc.* **187**, 158–172.

Wan, D.S., Rajadhyaksha, M. & Webb, R.H. (2000) Analysis of spherical aberration of a water immersion objective: application to specimens with refractive indices 1.33–1.40. *J. Microsc.* **197**, 274–284.

Weast, R.C., ed. (1989) *CRC Handbook of Chemistry and Physics.* CRC Press, Boca Raton, Florida.

Wilson, T., ed. (1990) *Confocal Microscopy.* Academic Press, London.

Wilson, T. & Sheppard, C.J.R. (1984) *Theory and Practice of Scanning Optical Microscopy.* Academic Press, London.

Fig. 9. Confocal axial response for focusing with an NA = 0.9 water immersion lens to nominal depths d_4 of (a) 200 μm; (b) 300 μm; and (c) 400 μm. The horizontal axis shows the setting of the correction collar in terms of the coverglass thickness.